2*T* domain-engineered piezoelectric single crystals: Calculations and application to PZN–12%PT poled along [101]

Mael Guennou,[1,a)] Hichem Dammak,[1] and Mai Pham Thi[2]
[1]*Laboratoire SPMS, UMR 8580 CNRS, École Centrale Paris, Grande Voie des Vignes, 92295 Châtenay-Malabry, France*
[2]*Thales Research and Technology France, 91767 Palaiseau, France*

(Received 17 April 2008; accepted 16 July 2008; published online 1 October 2008)

This work is devoted to a study of the [101] domain-engineered PZN–12%PT single crystals. The full electromechanical tensor of PZN–12%PT in its tetragonal single domain state 1*T* is determined by the resonance method and used as input data. Observations of the domain structure of the [101]-poled 2*T* crystals by polarized light microscopy reveal a laminar structure consisting of thin layers stacked along the macroscopic polarization direction. We give analytical expressions for effective constants of this laminate multidomain pattern, taking into account the clamping effect resulting from domain coexistence. The calculated effective properties are found in good agreement with the experiments within experimental uncertainties. It is found that domain coexistence affects primarily the transverse dielectric constants ε_{11} and ε_{22}. This effect is related to the emergence of internal shear stresses and depolarizing electric fields that are most significantly driven by the shear piezoelectric constant d_{15} and dielectric anisotropy $\varepsilon_{11}^T-\varepsilon_{33}^T$ of the single domain state. © *2008 American Institute of Physics*. [DOI: 10.1063/1.2978327]

I. INTRODUCTION

$Pb(Zn_{1/3}Nb_{2/3})O_3-xPbTiO_3$ and $Pb(Mg_{1/3}Nb_{2/3})O_3-xPbTiO_3$ single crystals have raised considerable interest for more than 20 years due to their excellent piezoelectric properties, which offer promising improvement perspectives for piezoelectric transducers and actuators. In those systems, the highest piezoelectric coefficients d_{33} are obtained for compositions close to the morphotropic phase boundary ($x\approx 9\%$ for PZN–*x*PT, 35% for PMN–*x*PT) when poled along a [001] direction.[1] Those so-called domain-engineered crystals exhibit a ferroelectric domain structure that determines their macroscopic properties.

Various approaches were proposed in order to calculate the effective properties of multidomain crystals. Multiscale finite element models have been developed (see, for example, Uetsuji *et al.*[2] for an application to $BaTiO_3$ and $PbTiO_3$ and references therein). Classical self-consistent homogenization methods have been extended to the piezoelectric case by Li[3] and applied to PZN–4,5%PT by Ahart *et al.*[4] Different calculations on laminar structures have been published over the past few years. Such a model has been presented by Erhart and Cao,[5] Li and Liu,[6] and used notably by the latter to calculate effective properties of $BaTiO_3$ poled along [111].[7] With a different structure hypothesis, Delaunay developed a model in a similar way and applied it to PMN–33%PT.[8] Recently, Rödel presented a review of such works as well as a general matrix formalism and applications to some special cases of simple and hierachical laminar domain patterns.[9]

Although the models give predictions in a variety of cases, there are relatively few comparisons with experimental data, which make it difficult to evaluate the relevance of the various approaches. Moreover, the calculations are often carried out for crystals in the morphotropic phase boundary, where the properties are extremely sensitive to composition and inhomogeneities, which makes the comparison with experiments hazardous. The aims of this study are therefore, (i) to provide a deeper insight into the effective properties of 2*T* domain structures and (ii) to provide experimental data for an evaluation of the relevance of the calculations. We focus on tetragonal PZN–12%PT poled along [101] since the electromechanical properties are less sensitive to chemical heterogeneity.

This paper is organized as follows: the experimental methods are presented in Sec. II including sample preparation in Sec. II A, optical observations in Sec. II B and determination of the electromechanical properties of the 1*T* and 2*T* domain states in Sec. II C. Section III is devoted to the calculation of the effective properties. The comparison between experiments and calculations is discussed in Sec. IV.

II. MEASUREMENTS AND OBSERVATIONS

A. Sample preparation

PZN–12%PT single crystals were grown by the flux method (PbO flux) as described elsewhere.[10] They are orientated using the Laue backscattering technique. Crystals are cut with a wiresaw along the set of directions [001]/[010]/[100] and [101]/[010]/[10$\bar{1}$] relative to the cubic axes with dimensions reaching the requirements for the resonance method.[11] Crystal faces are polished on silicon carbide disks with grain sizes down to 1 μm to obtain mirrorlike surfaces. Gold electrodes (not thicker than 0.15 μm) are sputtered on the relevant surfaces of the samples. Samples are then annealed at 400 °C for 2 h to release stress

[a)]Electronic mail: mael.guennou@ecp.fr.

 © 2008 American Institute of Physics

Downloaded 03 Oct 2008 to 138.195.90.19. Redistribution subject to AIP license or copyright; see http://jap.aip.org/jap/copyright.jsp

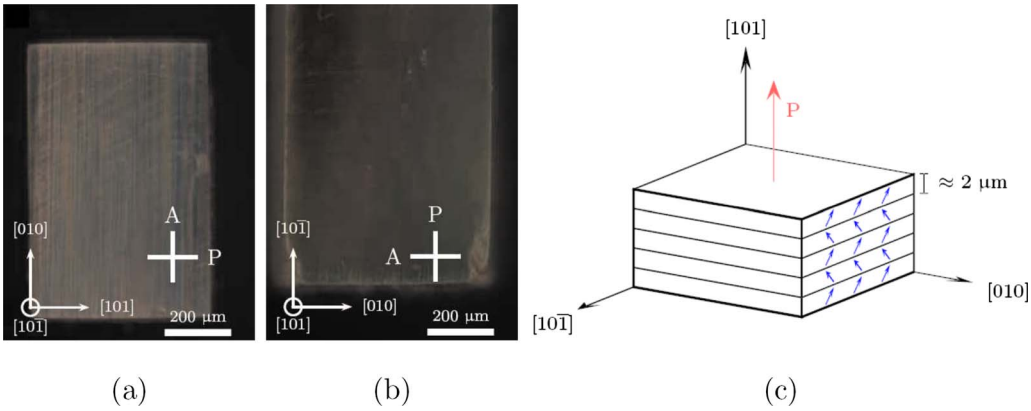

FIG. 1. (Color online) [(a) and (b)] Typical images from optical observations of [101]-poled multidomain single crystals. The directions of the crossed polarizers and analyzers are indicated by P and A, respectively. (c) Sketch of the $2T$ domain structure.

induced by polishing. The crystals are poled by the field cooling method whereby the sample is heated up into the cubic phase (490 K), an electric field is applied along a given crystallographic direction and the sample is slowly cooled down. For all samples, we used an electric field of 1 kV/cm and a cooling rate of 2 °C/min.

PZN–12%PT crystals are tetragonal with a spontaneous polarization lying along a [001] direction.[12] When poled along one of the six equivalent directions, the crystal is in a tetragonal single domain state labeled $1T$ with macroscopic symmetry $4mm$. We had previously shown that the single domain state could be unstable in plates thinner than 300 μm[13] and checked by optical microscopy that the polarization is homogeneous throughout the samples. When poled along a [101] direction, the crystal is in a tetragonal multidomain state $2T$ with two energetically equivalent polarization directions. A macroscopic symmetry $mm2$ is expected. In that case, the axes are labelled as follows: 3 is the macroscopic polarization direction, that is to say the [101] direction, the directions 1 and 2 refer to the [10$\bar{1}$] and [010] directions, respectively.

B. Polarized light microscopy

Figures 1(a) and 1(b) show typical micrographs of a multidomain $2T$ observed along and perpendicular to the macroscopic polarization. The observations along directions 1 and 2 (perpendicular to the macroscopic polarization) show a laminar structure with thin layers with thicknesses of a few microns. When observed along the polarization direction however, no structure is visible. In all cases, the crystals exhibit extinctions between the crossed polarizer and analyzer that are consistent with the expected polarization directions. We can therefore model the [101]-poled crystals as laminates with layers where the local polarization makes an angle of alternatively ±45° with the macroscopic polarization axis, as depicted in Fig. 1(c).

Since the layer thickness is much smaller than the crystal thickness, we can consider the crystal as a continous medium with $mm2$ macroscopic symmetry. Remarkably, this laminate is the most energetically favorable since (i) the spontaneous strains are compatible at the domain walls (ii) only uncharged domain walls are present.

C. Impedance measurements

Impedence measurements are carried out at room temperature with an impedance analyzer HP 4294A. The permittivity at constant stress is measured at 1 kHz. The results for all samples poled along [001] and [101] are given in Table I. Former results obtained by Zhang *et al.*[14] are reported for comparison. The agreement between our results and theirs are good, except for the k_{31} and d_{31} of the $2T$ samples where an explanation should be found. Since we find a higher coupling coefficient, we believe the poling of the crystal may be a possible cause for this discrepancy.

Crystals poled along [001] are in a tetragonal single domain state $1T$ with $4mm$ macroscopic symmetry. The electromechanical properties are then fully characterized by 11 independent coefficients. All those coefficients can be obtained by impedance measurements as detailed by Geng

TABLE I. Coupling coefficients, elastic compliances, and piezoelectric constants measured by the resonance method for PZN–12%PT poled along [001] (single domain state $1T$) and [101] (multidomain state $2T$). Measurements by Zhang *et al.* (Ref. 14) are reported for comparison.

	$P\parallel[001]$		$P\parallel[101]$	
	This work	Zhang *et al.*	This work	Zhang *et al.*
k_{31}	54.6 ± 2	54	42 ± 0.5	29.7
k_{32}			14 ± 0.5	14.5
k_{33}	87.8 ± 1	87	63 ± 0.5	61.5
k_{t33}	60.0 ± 1	55		
k_{15}	49.7 ± 3			
d_{31}	−207 ± 10	−207	−431 ± 10	−244
d_{32}			−136 ± 5	−121
d_{33}	541 ± 30	560	570 ± 10	530
d_{15}	653 ± 100			
s_{11}^E	20.1 ± 1	22.4	17.8 ± 0.3	16.6
s_{22}^E			19.2 ± 0.3	19.3
s_{33}^E	54.5 ± 4	58	15.8 ± 0.4	15.1
s_{12}^E	−4.6 ± 9			
s_{13}^E	−18.2 ± 7			
s_{44}^E	19.5 ± 4			
s_{66}^E	17.2 ± 19			
ε_{11}^T	10 000 ± 500		975 ± 50	
ε_{22}^T			6300 ± 300	
ε_{33}^T	750 ± 50	870	6000 ± 500	5500

Downloaded 03 Oct 2008 to 138.195.90.19. Redistribution subject to AIP license or copyright; see http://jap.aip.org/jap/copyright.jsp

et al.[15] We follow here the same procedure and report the full electromechanical tensor. We are however aware of the uncertainties arising from these measurements as underlined notably by Zhang *et al.*[16,17] It is clear from an uncertainty analysis that s_{12}^E and s_{66}^E should be taken with extreme precautions (relative uncertainty $>100\%$). It must be highlighted that a rather large uncertainty is attributed to the d_{15} coefficient due to the stringent conditions that the dimensions of the sample should fulfill.[18] The knowledge of those uncertainties will enable us to focus on the most reliable values and draw nevertheless significant conclusions.

Crystals poled along [101] are found to exhibit a $mm2$ macroscopic symmetry by optical observations. In that case, we only measured some of the 16 coefficients of the full electromechanical tensor. It should be reminded that the resonance method does not yield the sign of the piezoelectric constants. We chose positive signs for d_{33} and negative signs for d_{31} and d_{32}.

III. CALCULATION OF EFFECTIVE PROPERTIES

The general approach and hypothesis are presently briefly below. They are similar to those presented in the work published recently by Rödel[9] and we will not give any full derivation but send the reader to this reference for a full treatement of the problem in a convenient matrix formalism. In this paper, we intend to recall the basic hypothesis, develop further the special case of the $2T$ domain state, give analytical expressions of the effective constants when possible, and compare it to the measured values.

We choose the electric field E and the stresses T as independent variables. The electromechanical properties are therefore described by the dielectric constants at constant stress ε_{ij}^T, the elastic compliances at constant electric field $s_{\alpha\beta}^E$, and the piezoelectric constants $d_{i\alpha}$. Since there is no ambiguity, the superscripts E and T will be omitted for simplicity in the following.

In addition, we use the following notations: ε_{ij}^T, $d_{i\alpha}$, and $s_{\alpha\beta}$ are used for the values of the single domain state $1T$. The coefficients obtained by a rotation of 45° around the [010] axis are refered to as intrinsic properties and written ε_{ij}^{T*}, $d_{i\alpha}^*$, and $s_{\alpha\beta}^*$. The effective properties will be noted $\varepsilon_{ij}^{\text{eff}}$, $d_{i\alpha}^{\text{eff}}$, and $s_{\alpha\beta}^{\text{eff}}$.

The assumptions for this calculation are the following: (i) we consider a prefect laminate, (ii) the volume fractions of the two domain families are equal, and (iii) all fields are homogeneous within a domain. We do not take into account any movement of the domain walls. The tensor of the local electromechanical properties in a domain where the polarization is rotated by $\pm 45°$ around the [010] axis is given by

$$\begin{bmatrix} s_{11}^* & s_{12}^* & s_{13}^* & & \pm s_{15}^* & & \pm d_{11}^* & & d_{31}^* \\ s_{12}^* & s_{11}^* & s_{23}^* & & \pm s_{25}^* & & \pm d_{12}^* & & d_{32}^* \\ s_{13}^* & s_{23}^* & s_{33}^* & & \pm s_{35}^* & & \pm d_{13}^* & & d_{33}^* \\ & & & s_{44}^* & & \pm s_{46}^* & & d_{24}^* & \\ \pm s_{15}^* & \pm s_{25}^* & \pm s_{35}^* & & s_{55}^* & & d_{15}^* & & \pm d_{35}^* \\ & & & \pm s_{46}^* & & s_{66}^* & & \pm d_{26}^* & \\ \pm d_{11}^* & \pm d_{12}^* & d_{13}^* & & d_{15}^* & & \varepsilon_{11}^* & & \pm \varepsilon_{13}^* \\ & & & d_{24}^* & & \pm d_{26}^* & & \varepsilon_{22}^* & \\ d_{31}^* & d_{31}^* & d_{33}^* & & \pm d_{35}^* & & \pm \varepsilon_{13}^* & & \varepsilon_{33}^* \end{bmatrix}. \quad (1)$$

The expressions for some of those coefficients are given explicitely in the Appendix. The local properties within a domain do not respect the macroscopic symmetry $mm2$. However, the unwanted coefficients vanish under volume averaging with equal volume ratios. To calculate the effective properties in this way assumes that all stresses and electric fields T_α and E_i are homogeneous throughout the sample. This implies the existence of opposite strain or electric displacements in adjacent domains, which may not be allowed by the continuity conditions across the domain walls. If there is incompatibility, then the corresponding strains or electric displacements are clamped and opposite induced stress and electric fields emerge in the domains and contribute to the macroscopic response.

The orientation of the domain walls determine the field components that should remain continuous. We consider two template structures for $2T$ domain states depicted in Fig. 2.

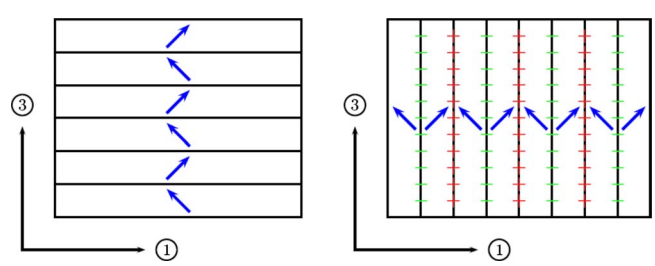

FIG. 2. (Color online) Sketches of an uncharged (left) and charged (right) domain wall structures with compatible spontaneous strains.

Downloaded 03 Oct 2008 to 138.195.90.19. Redistribution subject to AIP license or copyright; see http://jap.aip.org/jap/copyright.jsp

TABLE II. Analytical expressions for the effect of domain coexistence in perfect uncharged and charged structures. For a given coefficient a_{ij}, the expression given is the relative shift from the intrinsic value, that is to say, the G so that $a_{ij}^{\text{eff}}=a_{ij}^{*}(1+G)$.

Coefficient	Uncharged structure	Charged structure
$\varepsilon_{11}^{\text{eff}}$	(More complicated and therefore hardly usefull)	
$\varepsilon_{22}^{\text{eff}}$	$-\frac{d_{26}^{*2}}{\varepsilon_{22}^{*}s_{66}^{*}}=-\frac{d_{24}^{2}}{\varepsilon_{22}(s_{44}+s_{66})}$	0
$\varepsilon_{33}^{\text{eff}}$	0	$-\frac{\varepsilon_{13}^{*2}}{\varepsilon_{33}^{*}\varepsilon_{11}^{*}}=-\left(\frac{\varepsilon_{11}-\varepsilon_{33}}{\varepsilon_{11}+\varepsilon_{33}}\right)^{2}$
d_{31}^{eff}	0	$-\frac{d_{11}^{*}}{d_{31}^{*}}\frac{\varepsilon_{13}^{*}}{\varepsilon_{11}^{*}}=-\frac{-d_{31}-d_{33}-d_{15}}{d_{31}+d_{33}-d_{15}}\frac{\varepsilon_{11}-\varepsilon_{33}}{\varepsilon_{11}+\varepsilon_{33}}$
d_{32}^{eff}	0	$-\frac{d_{12}^{*}}{d_{32}^{*}}\frac{\varepsilon_{13}^{*}}{\varepsilon_{11}^{*}}=+\frac{\varepsilon_{11}-\varepsilon_{33}}{\varepsilon_{11}+\varepsilon_{33}}$
d_{33}^{eff}	0	$-\frac{d_{13}^{*}}{d_{33}^{*}}\frac{\varepsilon_{13}^{*}}{\varepsilon_{11}^{*}}=-\frac{-d_{31}-d_{33}+d_{15}}{d_{31}+d_{33}+d_{15}}\frac{\varepsilon_{11}-\varepsilon_{33}}{\varepsilon_{11}+\varepsilon_{33}}$
d_{24}^{eff}	$-\frac{d_{26}^{*}s_{46}^{*}}{d_{24}^{*}s_{66}^{*}}=-\frac{s_{44}-s_{66}}{s_{44}+s_{66}}$	0
s_{11}^{eff}	0	$-\frac{d_{11}^{*2}}{\varepsilon_{11}^{*}s_{11}^{*}}=-\frac{(d_{31}+d_{33}+d_{15})^{2}}{(\varepsilon_{11}+\varepsilon_{33})(s_{11}+2s_{13}+s_{33}+s_{55})}$
s_{22}^{eff}	0	$-\frac{d_{12}^{*2}}{\varepsilon_{11}^{*}s_{22}^{*}}=-\frac{d_{32}^{2}}{(\varepsilon_{11}+\varepsilon_{33})s_{22}}$
s_{33}^{eff}	0	$-\frac{d_{13}^{*2}}{\varepsilon_{11}^{*}s_{33}^{*}}=-\frac{(d_{31}+d_{33}-d_{15})^{2}}{(\varepsilon_{11}+\varepsilon_{33})(s_{11}+2s_{13}+s_{33}+s_{55})}$

In both cases, the spontaneous strains are compatible at the domain wall. In the first case however, the domain walls are uncharged domain wall and orthogonal to the 3 direction. In the second case, the domain walls are orthogonal to the 1 direction and are charged. We will refer to these structures as uncharged and charged structure, respectively.

For those two structures, we get simple analytical expression in a number of cases. Those correspond to cases where the incompatible strains or electric displacements are compensated by a single component of an electric field or stress only. The exact expressions are listed in Table II. In order to highlight the effect of domain coexistence, we write them as the relative difference to the intrinsic values, that is to say the G so that an effective constant a^{eff} is given by $a^{*}(1+G)$.

In many cases, an applied stress induces an internal electric field (or conversely). In such cases, the relation between the intrinsic coefficient and the effective coefficient is formally analog to the relation between s^{E} and s^{D} or ε^{T} and ε^{S}, where an electromechanical coupling coefficient k comes into play. An important exemple is the dielectric constant $\varepsilon_{22}^{\text{eff}}$ in the uncharged structure which is given by

$$\varepsilon_{22}^{\text{eff}}=\varepsilon_{22}^{*}\left[1-\frac{(d_{26}^{*})^{2}}{\varepsilon_{22}^{*}s_{66}^{*}}\right]=\varepsilon_{22}^{*}\left[1-\frac{d_{24}^{2}}{\varepsilon_{22}(s_{44}+s_{66})}\right]. \tag{2}$$

In that particular case, the effect comes from the emergence of opposite shear stresses T_6 in adjacent domains induced by the applied electric field E_2^{M} given by

TABLE III. PZN–12%PT poled along [101]: comparison between measured, intrinsic, and calculated values assuming an uncharged laminar structure.

	d_{31}	d_{32}	d_{33}	s_{11}	s_{22}	s_{33}	ε_{11}	ε_{22}	ε_{33}
a^{*}	−113	−146	349	14.5	20.4	14.5	5375	10 000	5375
a^{eff}	−113	−146	349	14.5	20.4	14.5	846	8690	5375
Measured	−431	−136	570	17.8	19.2	15.8	975	6300	6000

$$T_6^{\pm}=\mp\frac{d_{26}^{*}}{s_{66}^{*}}E_2^{M}. \tag{3}$$

For some cases, the applied stress in the sample induces internal stress only. Similarly, an applied electric field can induce internal electric fields only. In such cases, piezoelectricity effect does not come into play and the extrinsic effect only depends on the elastic (dielectric) properties alone. One such example is given by the effective dielectric constant ε_{33} in the charged structure

$$\varepsilon_{33}^{\text{eff}}=\varepsilon_{33}^{*}\left[1-\left(\frac{\varepsilon_{11}-\varepsilon_{33}}{\varepsilon_{11}+\varepsilon_{33}}\right)^{2}\right], \tag{4}$$

whereby the extrinsic effect arises from the emergence of an internal electric field

$$E_1^{\pm}=\mp\frac{\varepsilon_{13}^{*}}{\varepsilon_{11}^{*}}E_3^{M}. \tag{5}$$

As it could be expected, we notice that the effective dielectric constants and elastic compliances can only be reduced by the clamping effect. The piezoelectric coefficients however may be enhanced in the charged structure, depending on the ratios between the d_{31}, d_{32}, and d_{15} of the single domain state.

IV. DISCUSSION

We now move on to the comparison between intrinsic values, effective calculated values and actual measured values of the polydomain state $2T$. Consistent with the optical observations, we calculate the effective constants for an uncharged structure. In that case, among the nine constants measured, only $\varepsilon_{11}^{\text{eff}}$ and $\varepsilon_{22}^{\text{eff}}$ are expected to deviate from their intrinsic value. The comparison is presented in Table III.

Due to the uncertainties affecting some measured coefficients, not all calculated effective constants are equally reliable. Among the piezoelectric coefficients, the most reliable value is the d_{32}^{eff} which is simply given by $d_{32}^{*}=d_{31}/\sqrt{2}$. Both could be measured with a good accuracy and the agreement between measurement and calculation in that case is satisfactory. The elastic compliance s_{22} should also be checked first since $s_{22}^{*}=s_{22}$. We observe a small but acceptable difference.

As far as the dielectric constants are concerned, ε_{33} should remain equal to its intrinsic value while ε_{11} and ε_{22} are reduced by the domain coexistence. The measurements are qualitatively consistent with this prediction. Quantitatively, the calculation reproduces well the decrease in ε_{11} and ε_{22}, the agreement being especially good for ε_{11} where the

Downloaded 03 Oct 2008 to 138.195.90.19. Redistribution subject to AIP license or copyright; see http://jap.aip.org/jap/copyright.jsp

change is the most dramatic (reduced by more than 80%). A closer look on the latter case indicates that this comes from the emergence of stresses T_1 and T_2 and electric field E_3. Although the analytical expression is of little use, the analysis of the order of magnitudes indicates that the emergence of E_3 alone can account for more than 80% of the effect. The dielectric constant $\varepsilon_{11}^{\text{eff}}$ is then given to a good approximation by

$$\varepsilon_{11}^{\text{eff}} \approx \varepsilon_{11}^{*}\left[1-\left(\frac{\varepsilon_{11}-\varepsilon_{33}}{\varepsilon_{11}+\varepsilon_{33}}\right)^2\right] = 1400\varepsilon_0. \tag{6}$$

As mentioned earlier, this calculation does not take into account any extrinsic effect related to domain wall movements. In this special domain configuration, this effect would result in an increase in $\varepsilon_{11}^{\text{eff}}$.[19] The dramatic decrease measured here shows that this extrinsic effect, if it exists, is much less significant than the clamping effect, even if it cannot obviously be ruled out. Frequency or electric field dependent measurements could help to distinguish the two contributions.[20] The other constants discussed here, namely, $\varepsilon_{22}^{\text{eff}}$, $\varepsilon_{33}^{\text{eff}}$, d_{31}^{eff}, and d_{33}^{eff} are not expected to be affected by domain wall movement in this configuration.

It is remarkable that the most significant effects are driven by the shear piezoelectric coefficient d_{15} [as evidenced in Eq. (2)] and the dielectric anisotropy $(\varepsilon_{11}-\varepsilon_{33})$ of the single domain state. Both are related to the ability of the polarization to tilt away from its axis upon application of an electric field E_1. The very high d_{15} exhibited by the crystals close to the morphotropic phase boundary are also known to be responsible for the very high d_{33} in multidomain [001]-poled single crystals, like in PZN–9%PT[21] and PMN–33%PT.[22] It is therefore confirmed that this coefficient is the major feature of morphotropic crystals.

It is more difficult to draw conclusions from the values of other effective constants. The agreement is clearly unsatisfactory for the piezoelectric constants. However, this could be due to an error on the d_{15} coefficient which was the most difficult to measure. Similarly, it is difficult to give an interpretation for the disagreement between the calculated and measured values of s_{11}^{eff} and s_{33}^{eff} given the uncertainty affecting the s_{13} of the single domain state.

However, regardless of the absolute values of these coefficients, some more observations can be made. First of all, we notice that the equality $s_{11}^{\text{eff}}=s_{33}^{\text{eff}}$ holds in a perfect uncharged laminate. Yet, the compliances measured in our crystals are not equal. Also, in a perfect laminate, we have $d_{31}^{\text{eff}}+d_{33}^{\text{eff}}=d_{31}^{*}+d_{33}^{*}=(d_{31}+d_{33})/\sqrt{2}$. This can be easily checked since all the coefficients can be measured with good accuracy. The measured coefficients do not fulfill this condition, even within experimental errors (139 versus 236 pm/V). These differences show that the crystals cannot be regarded as perfect laminates. Domain wall movements alone cannot account for this since they are not supposed to affect any of the above mentioned coefficients. The presence of slightly disoriented and therefore somewhat charged domain walls might be the reason for this discrepancy.

V. CONCLUSION

We have measured the full electromechanical tensor of PZN–12%PT in its single domain state by the resonance method. Measurements of [101]-poled crystals were compared to effective properties calculated under the assumption that the crystals are perfect laminates. Analytical expressions were given in order to identify the relevance of the various coefficients in the magnitude of the extrinsic properties. The most significant extrinsic effect remains the dramatic decrease in $\varepsilon_{11}^{\text{eff}}$ and $\varepsilon_{22}^{\text{eff}}$, which is well accounted for by the calculations and found to be driven by the dielectric anisotropy $(\varepsilon_{11}-\varepsilon_{33})$ and the shear piezoelectric coefficient d_{15} of the single domain state, respectively, both related to the ability of the polarization to tilt away from its axis. On the other hand, we have given experimental evidence that the polydomain crystals are not perfect laminates. This study highlights the needs for a very precise determination of the electromechical properties of the single domain state in order to identify the different contributions in a multidomain state.

APPENDIX A: EXPRESSIONS

The expressions for the intrinsic properties for a single domain rotated by 45° as functions of the piezoelastic coefficient in the single domain state are

$$s_{11}^{*}=s_{33}^{*}=(s_{11}+s_{33}+2s_{13}+s_{55})/4,$$

$$s_{15}^{*}=(s_{11}-s_{33})/2,$$

$$s_{22}^{*}=s_{22},$$

$$s_{25}^{*}=s_{12}-s_{23},$$

$$s_{35}^{*}=(s_{11}-s_{33})/2,$$

$$s_{44}^{*}=(s_{44}+s_{66})/2,$$

$$s_{46}^{*}=(-s_{44}+s_{66})/2,$$

$$s_{55}^{*}=s_{11}-2s_{13}+s_{33},$$

$$s_{66}^{*}=(s_{44}+s_{66})/2,$$

$$\varepsilon_{11}^{*}=\varepsilon_{33}^{*}=(\varepsilon_{11}+\varepsilon_{33})/2,$$

$$\varepsilon_{22}^{*}=\varepsilon_{22},$$

$$d_{31}^{*}=(d_{31}+d_{33}-d_{15})/\sqrt{8};$$

$$d_{32}^{*}=d_{31}/\sqrt{2},$$

$$d_{33}^{*}=(d_{31}+d_{33}+d_{15})/\sqrt{8},$$

$$d_{11}^{*}=(-d_{31}-d_{33}-d_{15})/\sqrt{8},$$

$$d_{12}^{*}=-d_{32}/\sqrt{2},$$

Downloaded 03 Oct 2008 to 138.195.90.19. Redistribution subject to AIP license or copyright; see http://jap.aip.org/jap/copyright.jsp

$$d_{13}^{*} = (-d_{31} - d_{33} + d_{15})/\sqrt{8},$$

$$d_{35}^{*} = (d_{31} - d_{33})/\sqrt{2},$$

$$d_{15}^{*} = (-d_{31} + d_{33})/\sqrt{2},$$

$$d_{24}^{*} = d_{24}/\sqrt{2},$$

$$d_{26}^{*} = -d_{24}/\sqrt{2}.$$

[1] S.-E. Park and T. R. Shrout, IEEE Trans. Ultrason. Ferroelectr. Freq. Control **44**, 1997 (1997).
[2] Y. Uetsuji, Y. Nakamura, S. Ueda, and E. Nakamachi, Modell. Simul. Mater. Sci. Eng. **12**, S303 (2004).
[3] J. Y. Li, J. Mech. Phys. Solids **48**, 529 (2000).
[4] M. Ahart, A. Asthagiri, P. Dera, H.-K. Mao, R. E. Cohen, and R. J. Hemley, Appl. Phys. Lett. **88**, 042908 (2006).
[5] J. Erhart and W. Cao, J. Appl. Phys. **86**, 1073 (1999).
[6] J. Li and D. Liu, J. Mech. Phys. Solids **52**, 1719 (2004).
[7] D. Liu and J. Li, Appl. Phys. Lett. **83**, 1193 (2003).
[8] T. Delaunay, E. Le Clézio, M. Lematre, and G. Feuillard, IEEE Trans. Ultrason. Ferroelectr. Freq. Control **53**, 1974 (2006).
[9] J. Rödel, Mech. Mater. **39**, 302 (2007).
[10] A.-E. Renault, H. Dammak, G. Calvarin, M. Pham Thi, and P. Gaucher, Jpn. J. Appl. Phys., Part 1 **41**, 3846 (2002).
[11] IEEE, ANSI/IEEE Standard No. 176-1987.
[12] J. J. Lima-Silva, I. Guedes, J. Mendes Filho, A. P. Ayala, M. H. Lente, J. A. Eiras, and D. Garcia, Solid State Commun. **131**, 111 (2004).
[13] H. Dammak, M. Guennou, C. Ketchazo, M. Pham Thi, F. Brochin, T. Delaunay, P. Gaucher, E. Le Clézio, and G. Feuillard, Proceedings of the 15th IEEE International Symposium on Applications of Ferroelectrics, 2006 (unpublished), p. 249.
[14] S. Zhang, L. Lebrun, C. A. Randall, and T. R. Shrout, Phys. Status Solidi A **202**, 151 (2005).
[15] X. Geng, T. A. Ritter, and S. E. Park, Proceedings of the IEEE Ultrasonics Symposium, 1998 (unpublished), p. 571.
[16] R. Zhang, B. Jiang, W. Cao, and A. Amin, J. Mater. Sci. Lett. **21**, 1877 (2002).
[17] R. Zhang, B. Jiang, W. Jiang, and W. Cao, IEEE Trans. Ultrason. Ferroelectr. Freq. Control **49**, 1622 (2002).
[18] W. Cao, S. Zhu, and B. Jiang, J. Appl. Phys. **83**, 4415 (1998).
[19] R. Pérez, J. E. Garcia, A. Albareda, and D. A. Ochoa, J. Appl. Phys. **102**, 044117 (2007).
[20] D. Damjanovic, J. Am. Ceram. Soc. **88**, 2663 (2005).
[21] H. Dammak, A.-E. Renault, P. Gaucher, M. Pham Thi, and G. Calvarin, Jpn. J. Appl. Phys., Part 1 **42**, 6477 (2003).
[22] D. Damjanovic, M. Budimir, M. Davis, and N. Setter, Appl. Phys. Lett. **83**, 527 (2003).

Downloaded 03 Oct 2008 to 138.195.90.19. Redistribution subject to AIP license or copyright; see http://jap.aip.org/jap/copyright.jsp